Final Project Report

Theory and Applications of Computational Time-reversal Imaging

Anthony J. Devaney
Department of Electrical and Computer Engineering
Northeastern University
Boston, MA 02115

May 3, 2007

Abstract

This document constitutes the final project report for Contract # FA9550-04-1-0187 titled *Theory and Applications of Computational Time-reversal Imaging.* The report summarizes the theoretical development and implementation of time-reversal based imaging and target detection algorithms for locating targets from multistatic data collected from unstructured phased antenna arrays. The report summarizes the main theoretical results obtained in the program and includes both computer simulated examples as well as results from experimental data collected by a research team from Carnegie Mellon University illustrating the use of the algorithms developed in the project. The final section of the report outlines goals for follow-on research in these general areas.

Contents

REPORT DOCUMENTATION PAGE

Form Approved
OMB No. 0704-0188

1. REPORT DATE *(DD-MM-YYYY)*	2. REPORT TYPE	3. DATES COVERED *(From - To)*
14-12-2006	final	15-06-2004 to 14-09-06

4. TITLE AND SUBTITLE
Theory and Applications of Computational Time-reversal Imaging

5a. CONTRACT NUMBER

5b. GRANT NUMBER
FA9550-04-1-0187

5c. PROGRAM ELEMENT NUMBER

6. AUTHOR(S)
Anthony J. Devaney

5d. PROJECT NUMBER

5e. TASK NUMBER

5f. WORK UNIT NUMBER

7. PERFORMING ORGANIZATION NAME(S) AND ADDRESS(ES)

Division of Sponsored
Projects
Northeastern University
Boston, MA 02115

8. PERFORMING ORGANIZATION REPORT NUMBER

9. SPONSORING / MONITORING AGENCY NAME(S) AND ADDRESS(ES)
AFOSR
875 North Randolph St
Arlington, VA 22303-1768
Dr Arje Nachman/NE

10. SPONSOR/MONITOR'S ACRONYM(S)

11. SPONSOR/MONITOR'S REPORT NUMBER(S)

12. DISTRIBUTION / AVAILABILITY STATEMENT
Distribution Statement A: unlimited

AFRL-SR-AR-TR-07-0150

13. SUPPLEMENTARY NOTES

14. ABSTRACT
This document constitutes the final project report for Contract~\#~FA9550-04-1-0187 titled *Theory and Applications of Computational Time-reversal Imaging*. The report summarizes the theoretical development and implementation of time-reversal based imaging and target detection algorithms for locating targets from multi-static data collected from unstructured phased antenna arrays. The report summarizes the main theoretical results obtained in the program and includes both computer simulated examples as well as results from experimental data collected by Carnegie Mellon University illustrating the use of the algorithms developed in the project.

15. SUBJECT TERMS

16. SECURITY CLASSIFICATION OF:			17. LIMITATION OF ABSTRACT	18. NUMBER OF PAGES	19a. NAME OF RESPONSIBLE PERSON
a. REPORT	b. ABSTRACT	c. THIS PAGE			19b. TELEPHONE NUMBER *(include area code)*

1 Project Summary

The NU team consisted of myself as PI as well as Professors Hanoch Lev-Ari and Edwin Marengo (NU), Professor Arye Nehorai (UI) and Drs. Sean Lehman and David Chambers (LLNL). During this project the NU team was directed by DARPA to concentrate most of its effort on the problem of detecting a point target embedded in heavy clutter. They have modeled this problem *exactly* using the well-known *Foldy Lax equations* [1] that incorporate all multiple scattering between the targets, clutter and background and have proven [2] that the (non-linear) detection problem can be decomposed into the two *separate* problems of

1. Estimating the target/clutter locations using either classical time-reversal imaging (DORT) [11] or time reversal MUSIC [3, 4],

2. Estimating the target/clutter scattering amplitudes using a non-linear iterative algorithm developed in the study [5].

It is important to emphasize that even in the presence of multiple scattering the above two problems are independent; i.e., the target/clutter locations can be estimated using either time reversal DORT or MUSIC without knowing their scattering amplitudes. Once the target and clutter locations are known their scattering amplitudes are determined using a non-linear iterative algorithm that was also developed within the course of the project [5]. The final step in the detection problem is to use the computed target/clutter amplitudes in a maximum likelihood based detection algorithm. This time reversal based detection scheme has been tested and evaluated in extensive Monte Carlo computer simulations against other (linear) time reversal based detection schemes and against benchmark matched filter based schemes [6]. In all cases tested the time reversal approaches always outperform the matched

filter based methods and the non-linear time reversal based scheme developed in the project always came out best.

The target/clutter location estimation step is of key importance in the detection problem and the NU team has spent a good deal of effort on developing and testing alternative time reversal based imaging algorithms for performing this step. An important breakthrough in this investigation has recently been achieved when it was shown that time reversal MUSIC is only one of a large class of non-linear algorithms that allow point target/clutter locations to be estimated from the singular vectors of the SVD of the multistatic data matrix even in the presence of intense multiple scattering between targets and clutter. These generalized MUSIC algorithms are now being tested and evaluated on experimental data generated by a reserch team from Carnegie Mellon University (CMU) and a journal paper jointly authored by NU and CMU team members on this work is in preparation [7].

Besides developing, testing and evaluating time reversal based detection algorithms the NU team has also spent a good deal of effort developing time reversal based *inverse scattering algorithms* that yield *quantitative* estimates of distributed scatterers from multistatic scattered field data [8, 9, 10]. Thus, where time reversal DORT [11] and MUSIC [3, 4] and similar algorithms allow sets of isolated point scatterers to be imaged, the inverse scattering algorithms allow extended (3D) targets as well as the distributed background medium to be quantitatively determined. The estimation of backgrounds from scattered field data is extremely important within the context of the project since knowledge of the background allows the background Green function to be readily computed and used in the time reversal based detection algorithms developed in the study. It is important to mention that the inverse scattering algorithms developed in the study are based on the SVD of the mapping from the medium to the multistatic data and, hence, are extremely fast and efficient and can thus be incorporated into near real time applications.

An important part of the NU research was the development of more conventional approaches to the target detection problem [12, 13]. In particular, a number of maximum likelihood (ML) based detection schemes using standard signal processing techniques based on the time reversal scattering model for the multistatic data matrix were developed and evaluated in a Monte Carlo simulation study. One of these schemes, based on a single target scattering model, was employed as the benchmark algorithm for evaluation of the time reversal based algorithms developed in the program. This work was important since it showed that the time reversal based detection algorithms could be incorporated into the mathematical framework of conventional target detection theory and also because it laid the ground work of the extension of the time reversal based schemes to the stochastic framework that will be employed in Phase II of the project (see below).

2 Time reversed DORT and MUSIC Images

Much of the NU team effort was directed at *imaging* which is a first and crucial step in the target detection process. In imaging the acquired multistatic data is processed in such a way as to generate images of a set of targets from the scattered field data. We used three

schemes for generating these images:

1. Basic time reversal
2. The DORT method
3. Time reversal MUSIC

These three methods are described extensively in the literature cited at the end of the report. Images from both simulated as well as experimental data provided by Carnegie Mellon University (CMU) were employed in the study. In fact, the NU team were the first to successfully image the first CMU data set which was reported in a preliminary report titled "Basic Time Reversal Imaging of CMU Data Set," and which was issued early in the first year of the project. In the remainder of this section we first summarize the major results of that report and then present results obtained from subsequent CMU data sets obtained near the end of the project. All coding was done in Matlab and the codes with accompanying written reports were placed on the DARPA web site during the course of the project.

2.1 Early Results from CMU experimental data

Carnegie Mellon University (CMU) provided experimental test data on which the DARPA teams were required to apply their target imaging and detection algorithms. The experimental configuration is shown in fig. 1 and consists of a number of cylindrical targets whose radii were on the order of the EM wavelength used in the experiments. Multistatic data were acquired and made available to the various team members for test and evaluation of their algorithms. In the report cited above we used "basic time reversal imaging" to generate images of target sets from the first CMU data set acquired in the project. We first summarize how basic time reversal imaging is performed and then present the imaging results obtained in that report.

2.1.1 Basic Time Reversal Imaging

The basic method of time reversal imaging is simply to time reverse the scattered field measurements from all array sensor locations. At any given frequency this corresponds to the process of *field back propagation in the background medium* and is accomplished by conjugating the measured field amplitudes over the sensor locations and propagating the resulting amplitudes into the region containing the scatterers using the background Green

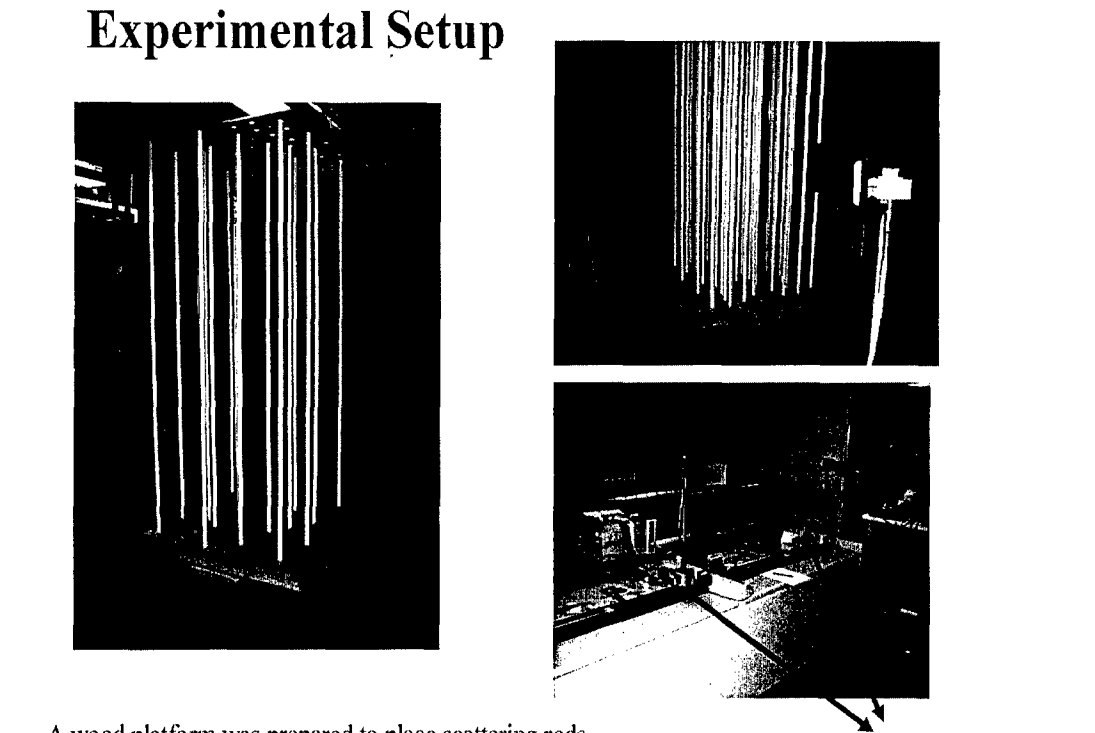

Figure 1: CMU experimental configuration.

function. Mathematically, this generates the time reversed (back propagated) field

$$\psi(\mathbf{x},\omega) = \sum_{j=1}^{N_\beta}\sum_{k=1}^{N_\alpha} K^*_{j,k}(\omega) G_0(\boldsymbol{\beta}_j,\mathbf{x},\omega) G_0(\boldsymbol{\alpha}_k,\mathbf{x},\omega) \tag{1a}$$

$$= \sum_{m=1}^{M} \tau_m(\omega)\{\sum_{j=1}^{N_\beta} G_0^*(\boldsymbol{\beta}_j,\mathbf{x}_m,\omega) G_0(\boldsymbol{\beta}_j,\mathbf{x},\omega)\}\{\sum_{k=1}^{N_\alpha} G_0^*(\boldsymbol{\alpha}_k,\mathbf{x}_m,\omega) G(\boldsymbol{\alpha}_k,\mathbf{x},\omega)\}$$

$$= \sum_{m=1}^{M} \tau_m(\omega) H_B(\mathbf{x},\mathbf{x}_m,\omega) H_A(\mathbf{x},\mathbf{x}_m,\omega), \tag{1b}$$

where

$$H_A(\mathbf{x},\mathbf{x}_m,\omega) = \sum_{k=1}^{N_\alpha} G_0^*(\boldsymbol{\alpha}_k,\mathbf{x}_m,\omega) G_0(\boldsymbol{\alpha}_k,\mathbf{x},\omega) \tag{2a}$$

$$H_B(\mathbf{x},\mathbf{x}_m,\omega) = \sum_{k=1}^{N_\beta} G_0^*(\boldsymbol{\beta}_j,\mathbf{x}_m,\omega) G(\boldsymbol{\beta}_j,\mathbf{x},\omega) \tag{2b}$$

are the transmit and receive *array point spread functions* (PSF's) , respectively[1]. At any given frequency the image field ψ formed from basic time reversal imaging from a set of point scatterers is seen to be equal to a sum of the product of the array PSF's weighted by the scatterers' reflection coefficients all centered at the scatterer locations.

2.1.2 Time Domain Field

The product of the transmit and receive array PSF's $H_A(\mathbf{x},\mathbf{x}_m,\omega)H_B(\mathbf{x},\mathbf{x}_m,\omega)$ will peak at the scatterer locations $\mathbf{x} = \mathbf{x}_m$ so that the peaks in the magnitude of the time reversed field ψ give an estimate of the locations of the various scatterers; i.e., will peak at the various scatterer locations $\mathbf{x}_m$, $m = 1, 2, \cdots, M$. The resolution of this basic scheme for estimating target location can be improved, especially, in backscatter measurements such as is the case for the CMU data, by integrating the field amplitude over the frequency band of the data. In particular,

$$\mathcal{H}_{A,B}(\mathbf{x},\mathbf{x}_m,t) = \frac{1}{2\pi}\int_{-\infty}^{\infty} d\omega\, H_{A,B}(\mathbf{x},\mathbf{x}_m,\omega) e^{-i\omega t}$$

will achieve its peak value at $t = 0$ so that the time domain time reversed field evaluated at $t = 0$ will yield optimum resolution of the various scatterer locations. This quantity is given by

$$\Psi(\mathbf{x}) = \frac{1}{2\pi}\int_{-\infty}^{\infty} d\omega\, \psi(\mathbf{x},\omega) = \frac{1}{2\pi}\int_{-\infty}^{\infty} d\omega \sum_{j=1}^{N_\beta}\sum_{k=1}^{N_\alpha} K^*_{j,k}(\omega) G_0(\boldsymbol{\beta}_j,\mathbf{x},\omega) G_0(\boldsymbol{\alpha}_k,\mathbf{x},\omega).$$

[1]Note that H_A only involves the background Green function while H_B involves both the background as well as the full Green functions. It can be shown that the peaks of both G_0 and G are, however, always occur at the point $\mathbf{x} = \mathbf{x}_m$; i.e., at the target location.

$$\Psi(\mathbf{x}) = \sum_{\omega_n} \sum_{j=1}^{N_\beta} \sum_{k=1}^{N_\alpha} K^*_{j,k}(\omega_n) G_0(\boldsymbol{\beta}_j, \mathbf{x}, \omega_n) G_0(\boldsymbol{\alpha}_k, \mathbf{x}, \omega_n)$$

2.2 Processed Image Data from first CMU data set

We processed all of the first CMU data set using both the basic time reversal imaging scheme described above as well as an SVD scheme described in the early report and useful for well resolved scatterers. We present in figures 2-5 the results obtained using the basic time reversal imaging scheme. The images were generated using the code cmu1.m which we placed on the DARPA web site.

2.3 Processed Images from later CMU data sets

We show in fig. 6 a schematic diagram of the CMU experimental configuration used in a number of the later tests. In data set # 11 a total of 17 dielectric rods were used as targets while in data set # 12 a conducting rod was added to the configuration. We imaged first the dielectric rods, then the dielectric rods plus conducting rod then finally processed the difference data to generate a final image of the conducting rod alone. The imaging results for standard time reversal imaging are shown in fig. 7 and those obtained using time reversal MUSIC are shown in fig. 8. The two are compared in fig. 9.

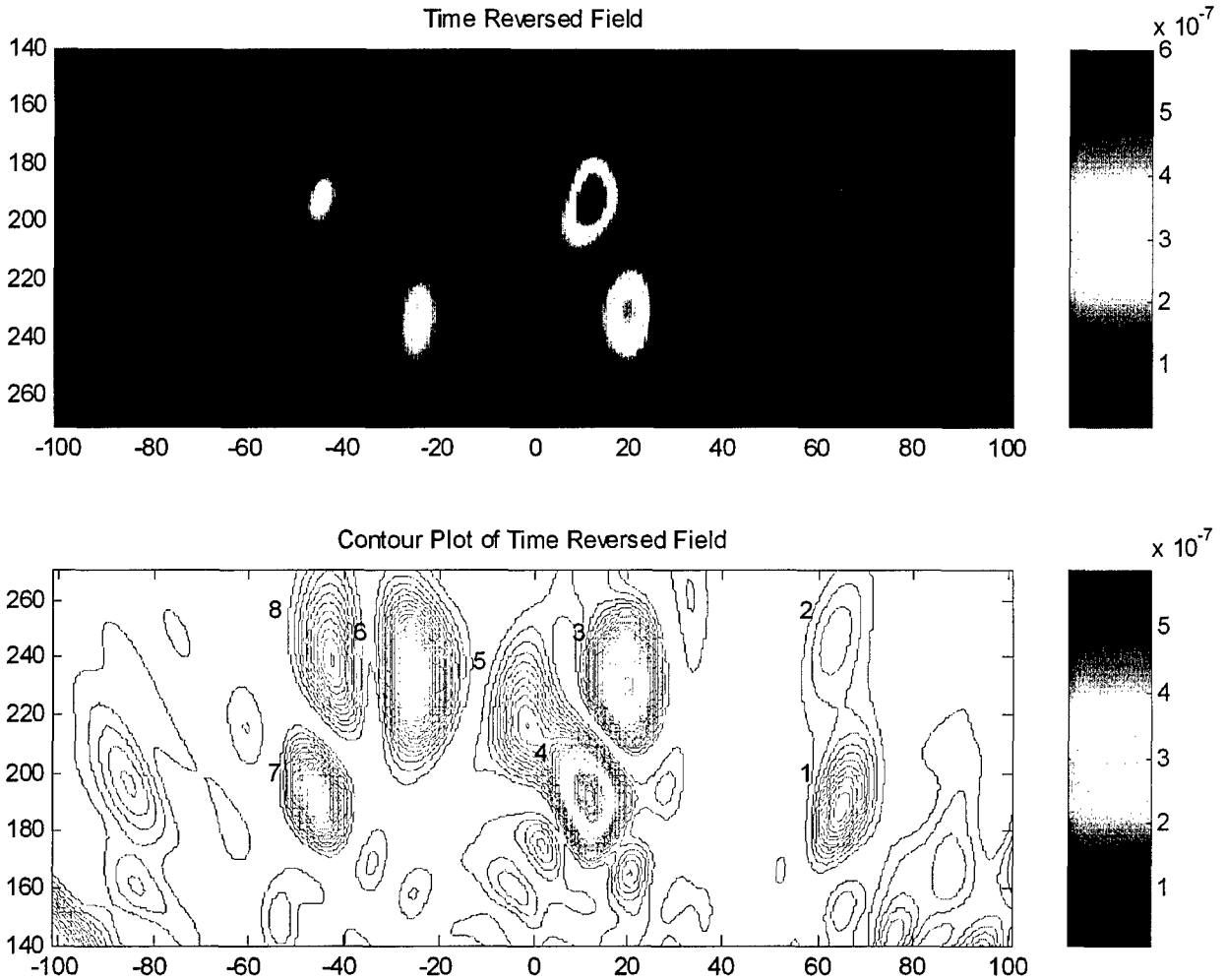

Figure 2: Time reversed field from eight scatterers processed at a single frequency equal to 5 MHz. The number of the scatterer is illustrated in both figures and the x,y axes are in centimeters. Note that due to the quirks of Matlab that the contour plot is drawn on an inverted vertical axis.

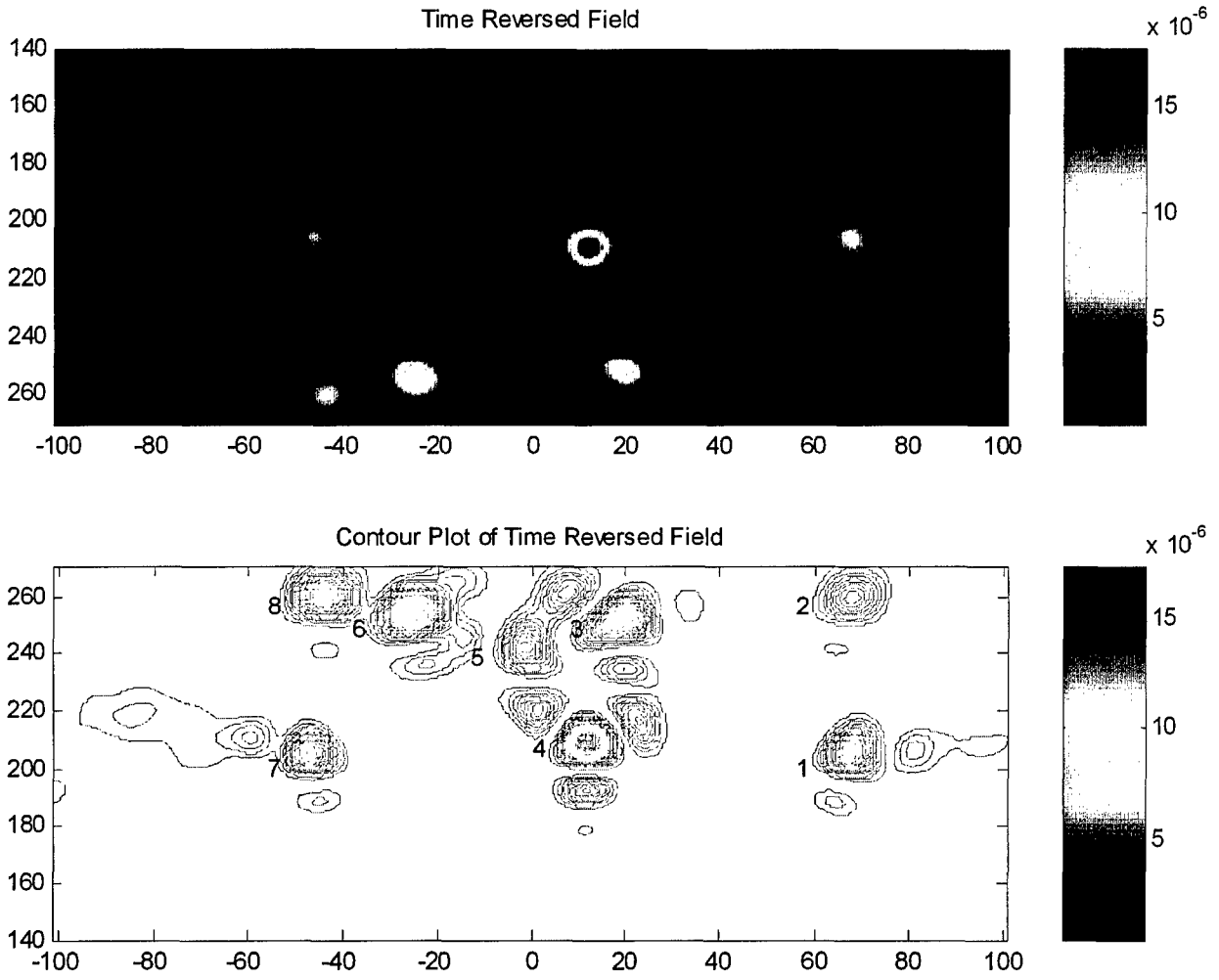

Figure 3: Time reversed field from eight scatterers processed at ten frequencies equally spaced between 4.5 and 5.5 MHz. The number of the scatterer is illustrated in both figures and the x,y axes are in centimeters. Note that due to the quirks of Matlab that the contour plot is drawn on an inverted vertical axis.

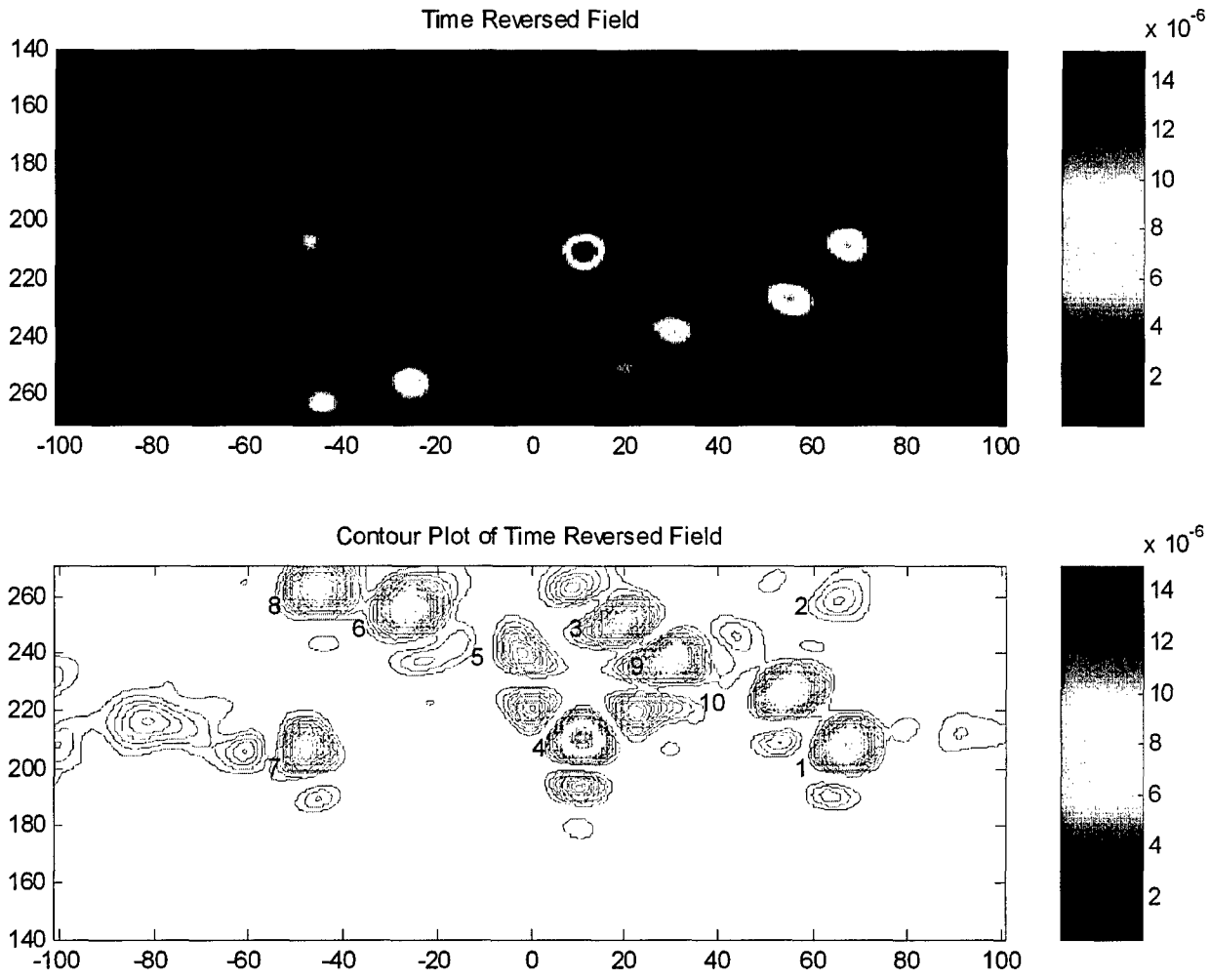

Figure 4: Time reversed field from ten scatterers processed at ten frequencies equally spaced between 4.5 and 5.5 MHz. The number of the scatterer is illustrated in both figures and the x,y axes are in centimeters. Note that due to the quirks of Matlab that the contour plot is drawn on an inverted vertical axis.

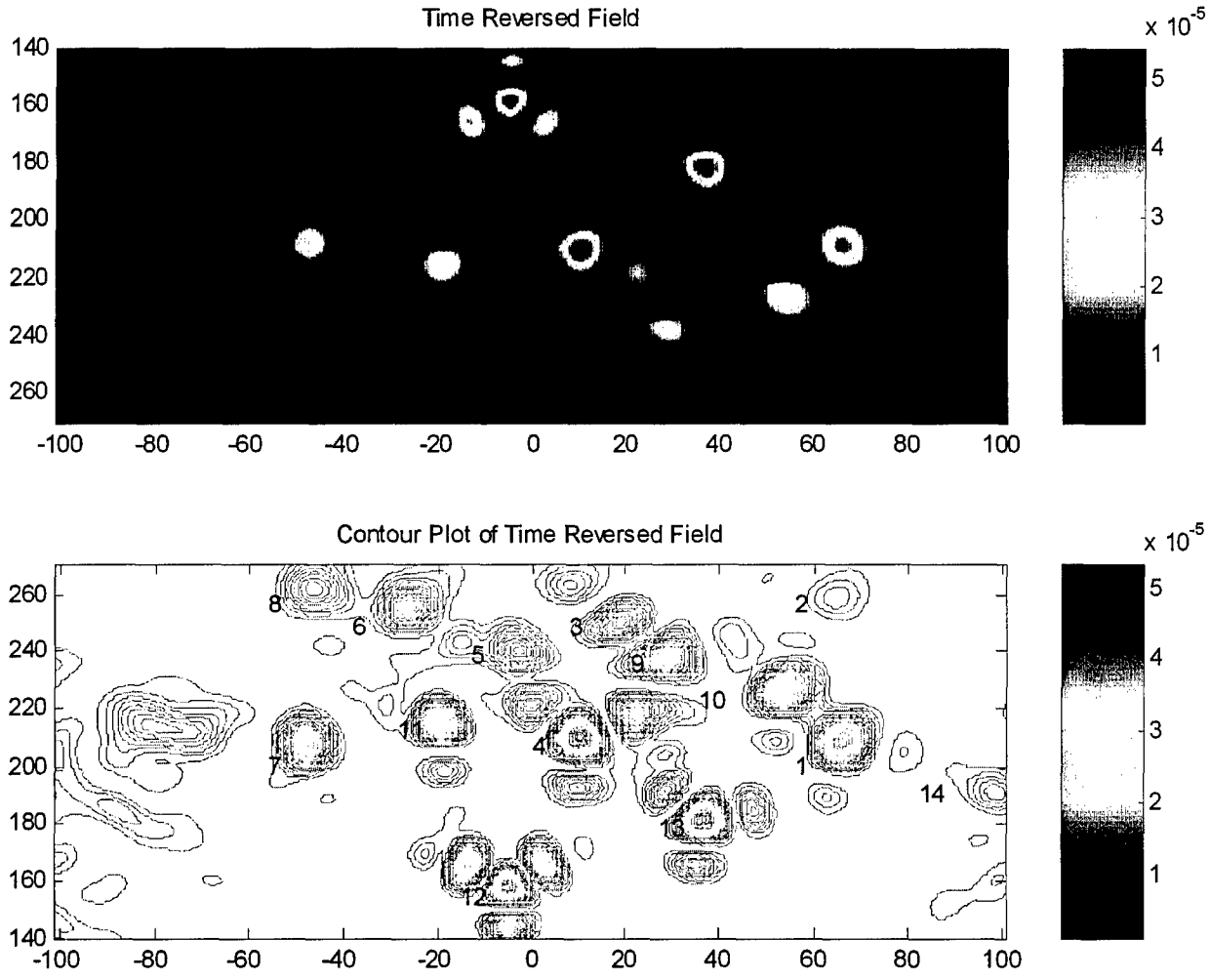

Figure 5: Time reversed field from fourteen scatterers processed at twenty frequencies equally spaced between 4.5 and 5.5 MHz. The number of the scatterer is illustrated in both figures and the x,y axes are in centimeters. Note that due to the quirks of matlab that the contour plot is drawn on an inverted vertical axis.

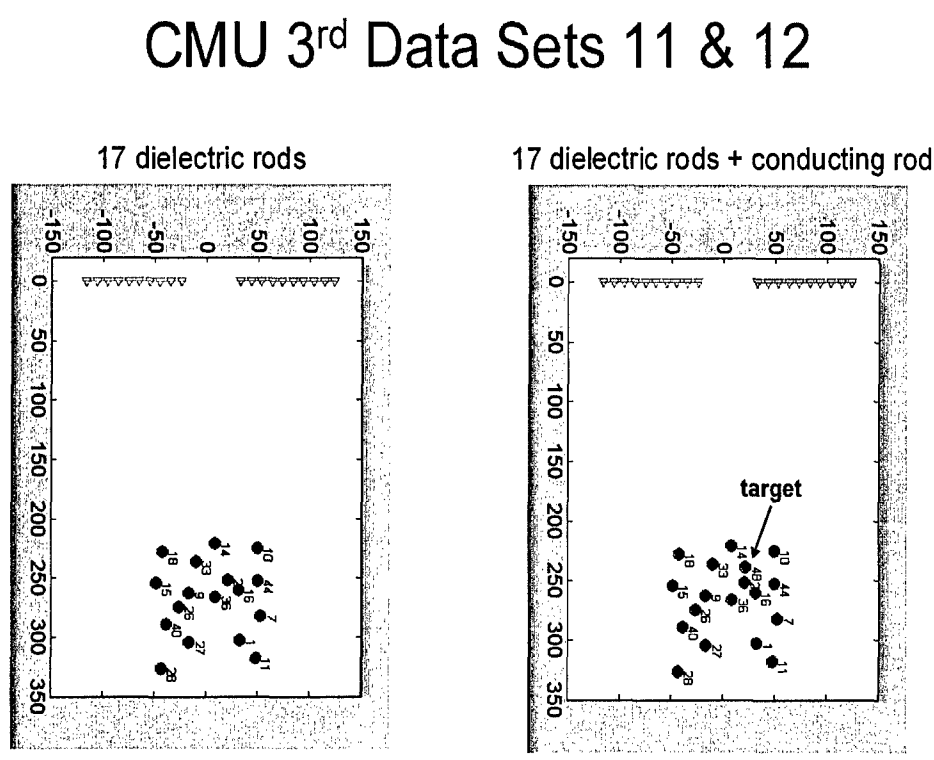

Figure 6: Scatterer and Antenna configurations for CMU experimental data for CMU Set #3 Setups 11 and 12.

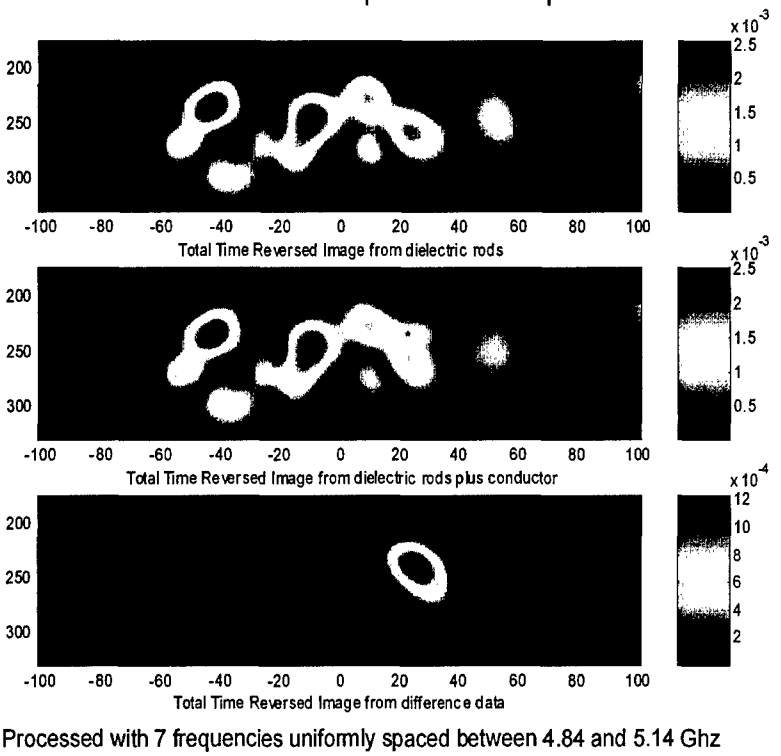

Figure 7: Total time reversed images from Experimental Set #3 Setups 11 and 12.

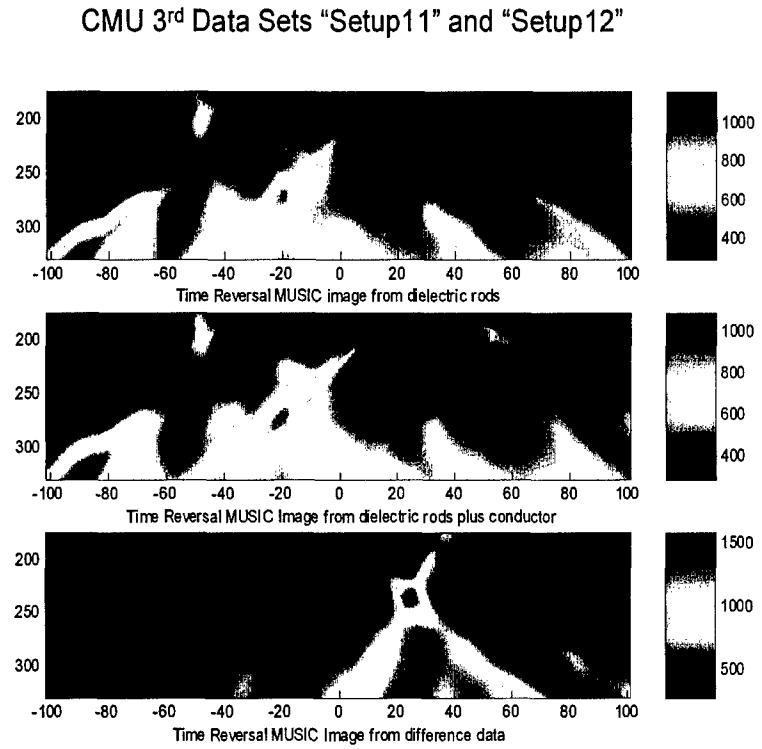

Figure 8: Time reversal MUSIC images from Experimental Set #3 Setups 11 and 12.

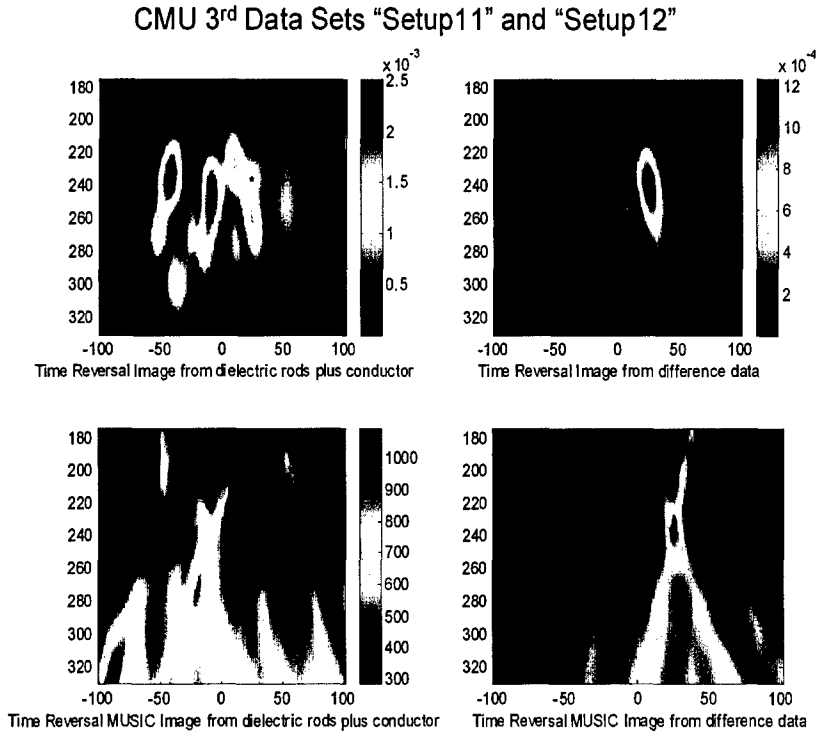

Figure 9: Comparison of Time reversal and Time reversal MUSIC images from Experimental Set #3 Setups 11 and 12.

3 DARPA Test Simulations

As mentioned earlier, one of the main objectives of this program was the detection of single or multiple point targets embedded in heavy clutter. The NU team employed an exact scattering model for this problem and first evaluated this model in computer simulations. We present in this section the results of the earliest such study which was a Monte Carlo test simulation consisting of the detection of a single point target embedded in the presence of a number of point clutter targets. The simulation tests the performance of two time reversal based detection algorithms; one based on the use of the distorted wave Born approximation (DWBA) for the K matrix and a second using a full multiple scattering based model for the K matrix [2, 5]. The details of the simulation code are reviewed and a few examples of the ROC and other performance curves resulting from the code are presented.

3.1 Synthetic Data Generation

We wish to compute a single realization of the measurement of the K matrix for a system of one dominant point target in the presence of $M_c < N-1$ clutter targets within a background whose Green function G_0 is known. We, of course, want to include all multiple scattering between the scatterers in the computation. The locations $\mathbf{x}_m, m = 0, 1, \cdots, M_c$ of the target and clutter are random variables uniformly distributed within a square with edge length L_x which is a free parameter in the simulation code. The scattering amplitude of the target τ_0 is randomly chosen to be either 0 or unity (equally probable) and the clutter scattering amplitudes $\tau_m, m = 1, 2, \cdots, M_c$ are taken to be zero mean Gaussian having a standard deviation σ_m that is also a free parameter. The simulation code works at a single frequency ω which will be assumed to be fixed throughout the following discussion. The frequency is fixed in the code by the use of a background wavelength λ which is set to unity. All lengths in the code are then given in wavelength units.

For any given realization of the scattering center locations $\{\mathbf{x}_m\}$ and scattering and target strengths $\{\tau_m\}$ the code generates synthetic data using the Foldy Lax equations [1]

$$G(\mathbf{x}_m, \boldsymbol{\alpha}_k, \omega) = G_0(\mathbf{x}_m, \boldsymbol{\alpha}_k, \omega) + \sum_{m' \neq m} \tau_{m'}(\omega) G_0(\mathbf{x}_m, \mathbf{x}_{m'}, \omega) G(\mathbf{x}_{m'}, \boldsymbol{\alpha}_k, \omega) \tag{3a}$$

where the antenna element locations $\boldsymbol{\alpha}_k$, $k = 1, 2, \cdots, N$ are also free parameters in the simulation code. The Foldy Lax equations are solved iteratively and the resulting full Green function $G(\mathbf{x}_m, \boldsymbol{\alpha}_k, \omega)$ is then used to compute the (noise free) multistatic data matrix according to its definition

$$K_{j,k}(\omega) = \sum_{m=0}^{M_c} \tau_m(\omega) G_0(\boldsymbol{\alpha}_j, \mathbf{x}_m, \omega) G(\mathbf{x}_m, \boldsymbol{\alpha}_k, \omega) \tag{3b}$$

The final step in the data generation process is the addition of additive noise to the computed multistatic data matrix according to the equation

$$\hat{K}_{j,k}(\omega) = K_{j,k}(\omega) + \text{Max } |K_{j,k}| \mathcal{N}_{j,k}(0, \sigma_W) e^{i\phi_{j,k}} \tag{4}$$

where $\mathcal{N}_{j,k}(0, \sigma_W)$ is a random matrix whose elements are uncorrelated and zero mean Gaussian with standard deviation equal to σ_W and where $\phi_{j,k}$ is an uncorrelated random matrix whose elements are uniformly distributed between 0 and 2π. The noisy K matrix $\hat{K}$ is then input into the time reversal based target detection algorithms described below.

3.2 Time Reversal MUSIC

Both of the time reversal based algorithms described below are assumed to have a first step that consists of estimation of all the scattering centers $\{\mathbf{x}_m\}$ (this includes target plus clutter). We showed previously that as long as the number of scattering centers $M = M_c + 1$ is less than the number of antenna elements N that this can be accomplished with time reversal MUSIC using the background Green function and the singular vectors v_p, $\sigma_p = 0$ where $Kv_p = \sigma_p u_p$ [3, 4, 15]. We assume here that this step is performed exactly by both of the algorithms discussed below.

3.3 Scattering Strength Estimation

Once the scattering centers are estimated (assumed known in the current Monte Carlo simulation code) the scattering strengths $\tau_m, m = 0, 1, \cdots, M_c$ are estimated. We used two procedures for doing this: one based on the DWBA model for the multistatic data matrix and a second based on the full multiple scattering model for this quantity. Thus, we are, in fact, using two time reversal algorithms: one based on the DWBA and a second on the full multiple scattering model using the Foldy Lax equations. We compared both of these algorithms with a standard "benchmark" algorithm in our work with the CMU data presented later in the report.

3.3.1 DWBA Based Algorithm

The DWBA algorithm employs the DWBA model for the multistatic data matrix for a system of N antennas located at $\boldsymbol{\alpha}_j$, $j = 1, 2, \cdots, N$ and $M = M_c + 1$ point scatterers located at $\mathbf{x}_m$, $m = 0, 1, 2, \cdots, M_c$, where, as above, M_c is the number of clutter targets:

$$K^b_{j,k} = \sum_{m=0}^{M_c} \tau_m(\omega) G_0(\boldsymbol{\alpha}_j, \mathbf{x}_m, \omega) G_0(\mathbf{x}_m, \boldsymbol{\alpha}_k, \omega), \tag{5}$$

where we have used the superscript "b" to denote the DWBA (Born) model for the K matrix. We write the above set of equations in the form

$$K^b_{j,k} = \sum_{m=0}^{M_c} G_0(\boldsymbol{\alpha}_j, \mathbf{x}_m, \omega) A_m(k) \tag{6a}$$

where

$$A_m(k) = \tau_m(\omega) G_0(\mathbf{x}_m, \boldsymbol{\alpha}_k, \omega). \tag{6b}$$

Eqs(6a) are a set of N^2 equations for the $N \times M$ unknowns $A_m(k)$, $m = 0, 1, \cdots, M_c$, $k = 1, 2, \cdots, N$. In the code the $K^b_{j,k}$ is set equal to the computed noisy K matrix $\hat{K}_{j,k}$ and a least squares solution of Eqs.(6a) is obtained for each value of $k = 1, 2, \cdot, N$. The final step is the estimation of the scattering coefficients which, in the DWBA model, are computed using the algorithm

$$\hat{\tau}_m = \frac{1}{N} \sum_{k=1}^{N} \frac{\hat{A}_m(k)}{G_0(\mathbf{x}_m, \boldsymbol{\alpha}_k, \omega)} \tag{7}$$

which is simply the an average of the N values of τ_m given according to Eq.(6b).

3.3.2 Multiple Scattering Based Algorithm

The multiple scattering based time reversal detection algorithm uses the exact multiple scattering model Eq.(3b) for the multistatic data matrix. This algorithm differs from the DWBA algorithm described above only in the definition of the quantities $A_m(k)$ and in the computation of the scattering strengths from the least squares solution of the set Eqs.(6a) (with, of course, $K^b_{j,k}$ set equal to the noisy measured K matrix $\hat{K}_{j,k}$). In particular, in place of Eq.(6b), the amplitudes $A_m(k)$ in the multiple scattering model are defined by

$$A_m(k) = \tau_m(\omega) G(\mathbf{x}_m, \boldsymbol{\alpha}_k, \omega). \tag{8a}$$

where G is the full Green function and must satisfy the Foldy Lax equations Eqs.(3a). In terms of $A_m(k)$ these equations can be written in the form

$$G(\mathbf{x}_m, \boldsymbol{\alpha}_k, \omega) = G_0(\mathbf{x}_m, \boldsymbol{\alpha}_k, \omega) + \sum_{m' \neq m} G_0(\mathbf{x}_m, \mathbf{x}_{m'}, \omega) A_{m'}(k). \tag{8b}$$

The multiple scattering based algorithm thus first uses a least squares solution of the set Eqs.(6a) which are then input into the Foldy Lax equations Eqs.(8b) to compute an estimate $\hat{G}$ of the full Green function $G(\mathbf{x}_m, \boldsymbol{\alpha}_k, \omega)$. The scattering strengths are then estimated via the equation

$$\hat{\tau}_m = \frac{1}{N} \sum_{k=1}^{N} \frac{\hat{A}_m(k)}{\hat{G}(\mathbf{x}_m, \boldsymbol{\alpha}_k, \omega)}, \tag{9}$$

which is seen to differ form the DWBA solution Eq.(7) only in the replacement of the background Green function G_0 with the (estimated) full Green function $\hat{G}$.

3.4 Detection Algorithms

The first processing step for both algorithms is target location estimation via MUSIC. This is a non-linear step which makes the remaining estimation step of the scattering strengths itself non-linear so that it is not possible to determine an "optimum" detection algorithm. However, if we make the simplifying assumption that this first step is exact (which is a reasonable assumption since MUSIC does perform very well) the estimation of the scattering

strengths for the DWBA algorithm is linear and an optimum algorithm can then be devised[2]. However, the same is not true for the multiple scattering based algorithm since the Foldy Lax equations are non-linear with the result that the estimation of the full Green function and target scattering strengths is a non-linear process. However, for the sake of simplicity we decided to use a simple threshold based algorithm for the detection step in both algorithms. Such an algorithm would only be appropriate for a linear model with AWGN but is used here for lack of anything better.

3.4.1 Threshold Test

In any given iteration (realization of random parameters) the Monte Carlo code generates two solution vectors $\hat{\tau} = [\hat{\tau}_0, \hat{\tau}_1, \cdots, \hat{\tau}_{M_c}]$ of the target scattering strengths (one using the DWBA algorithm and one using the multiple scattering based algorithm described above). The actual target strength is τ_0 and the remaining estimates are of the clutter amplitudes $\tau_m, m = 1, 2, \cdots, M_c$. Both the DWBA as well as the multiple scattering based algorithm make a decision by comparing the maximum value of the real part of the estimated solution vectors $J = \text{Max } \Re(\hat{\tau})$with a threshold T and deciding that the target is present if $J > T$ and not present if $J < T$. The probabilities of detection P_d and false alarm P_f are then computed from these results in a standard fashion by keeping track of correct and incorrect decisions. Plots of P_d and P_f as a function of the threshold value T are then generated as is a plot of the Receiver Operation Curve (ROC) which is simply a plot of P_d versus P_f.

3.5 Examples

To illustrate the Monte Carlo program we show a few examples that compare the performance of the DWBA based detection algorithm with the multiple scattering based algorithm. In these and later studies the figures are presented in the last section of the report. In all of these examples a linear array of $N = 6$ unequally spaced antenna elements were employed and $M_c = 4$ clutter targets and one single real target were used. The target and clutter locations were uniformly distributed within a square of length L_x which is labeled on the figures presented in the last section of the report. The center of the target/clutter support square was 32 wavelengths from the antenna array.

In Fig. 10 we show curves of the probabilities of detection P_d and false alarm P_f plotted versus threshold value T for one set of simulation parameters. In these and the following examples, the target has a scattering strength τ_0 that is equally probable to be unity (target present) or zero (no target) and the clutter targets were independent Gaussian random variables having zero mean and standard deviation σ_τ that is labeled on the figures. Also labeled on the figures are the number of Monte Carlo runs, the noise standard deviation σ_W (see Eq.(4)), and the length of the side of the support square for targets and clutter in

[2]This is possible since both the additive noise as well as the clutter amplitudes are Gaussian. This algorithm will, of course, be optimum only within the DWBA model and does not account for multiple scattering effects.

number of wavelengths. The ROC curves corresponding to the results shown in Fig. 10 are presented in Fig. 11.

It is seen from Fig. 10 that the probability of detection differs significantly for the two algorithms but that the false alarm probabilities are almost identical. This same trend was found in all simulations that were performed and so we only show the ROC curves for the later examples. It is clear from both Figs. 10 and 11 that the multiple scattering based algorithm clearly out performs the DWBA based algorithm. This is due to the fact that the targets and clutter are closely packed (within a square having sides of length $L_x = 3.2\ \lambda$ and that the clutter amplitudes are relatively large ($\sigma_\tau = 0.4$).

The ROC curves for the same set of parameters as used in the first example but with a different additive noise standard deviation are shown in Fig. 12. The increase in additive antenna noise clearly degrades the performance of both algorithms but is most strongly felt by the multiple scattering algorithm. This is probably due to error introduced into the estimation of the full Green function from the set of Eqs.(8b) due to error in the coefficients $A_m(k)$. Other simulations (not shown) indicate that this trend increases; i.e., the multiple scattering based algorithm is more sensitive to additive antenna noise than is the DWBA based algorithm.

In the final example the additive noise is again reduced to the level of the first example but the standard deviation of the clutter target amplitudes is increased. Again the multiple scattering algorithm out performs the DWBA based algorithm but the performance of both algorithms degrade relative to the performance in the first example. This is obviously due to false estimates of target presence due to the use of a simple threshold based detection algorithm; i.e., the maximum value of the estimated τ vector is more likely due to a high amplitude clutter target.

4 Monte Carlo Simulation from CMU Experimental Data

Carnegie Mellon University (CMU) provided experimental test data on which the DARPA teams were required to apply their target detection algorithms. The experimental configuration is shown in fig. 1 and consists of a number of cylindrical targets whose radii were on the order of the EM wavelength used in the experiments. Multistatic data were acquired and made available to the various team members for test and evaluation of their algorithms.

4.1 Signal Model

The third CMU data set was used to generate ROC curves using a *change detection* based signal model. In this study we used the experimentally obtained multistatic data matrix $K^{s+c}_{j,k}(\omega)$ corresponding to a given set of clutter targets plus a single copper target and the experimentally obtained multistatic data matrix $K^{c}_{j,k}(\omega)$ corresponding to only the clutter targets at the single frequency of 5 Ghz. The study assumed that a noisy version of the

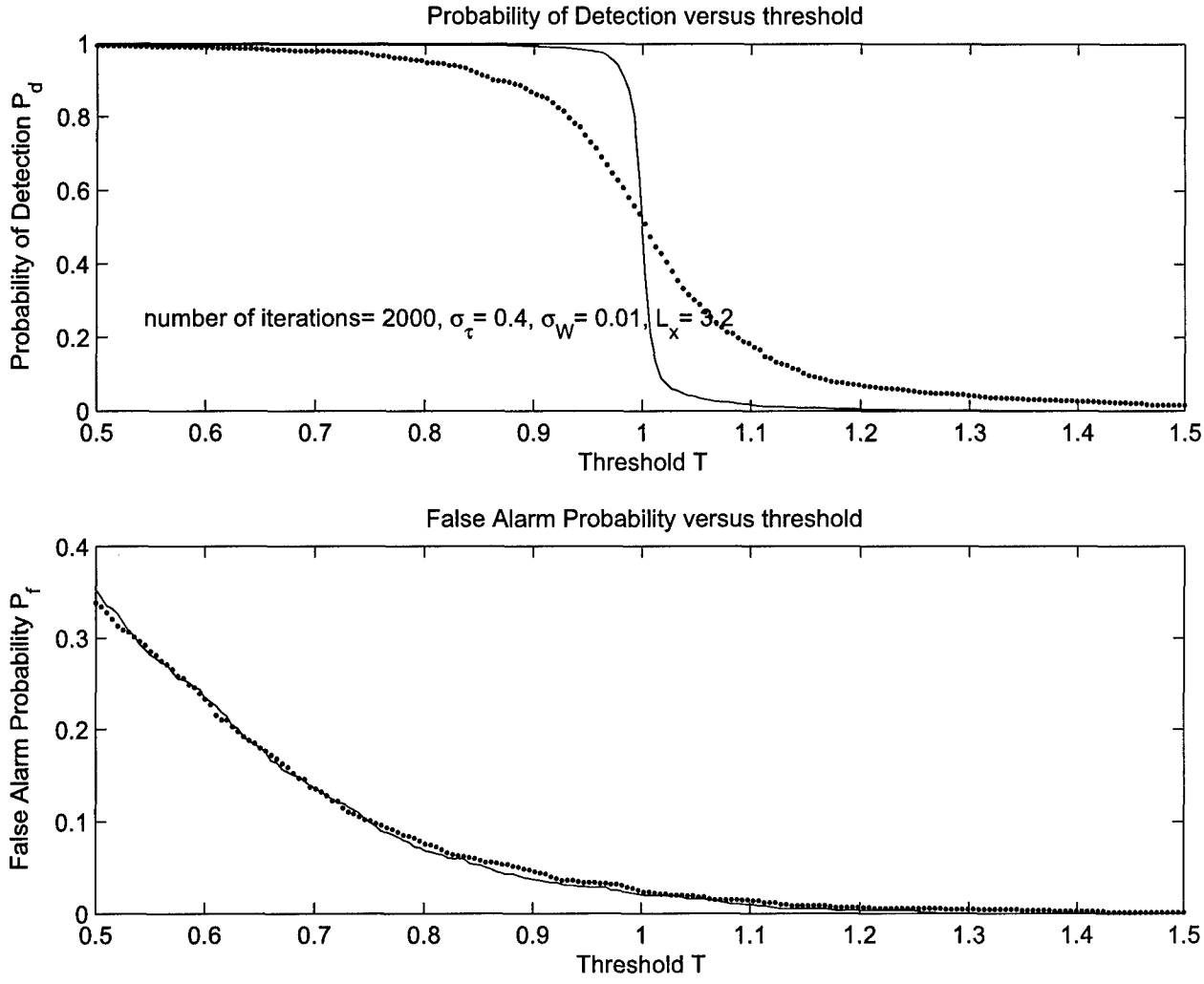

Figure 10: Plots of Probabilities of detection and false alarm for the DWBA (dotted) and multiple scattering based (solid) algorithms versus threshold value.

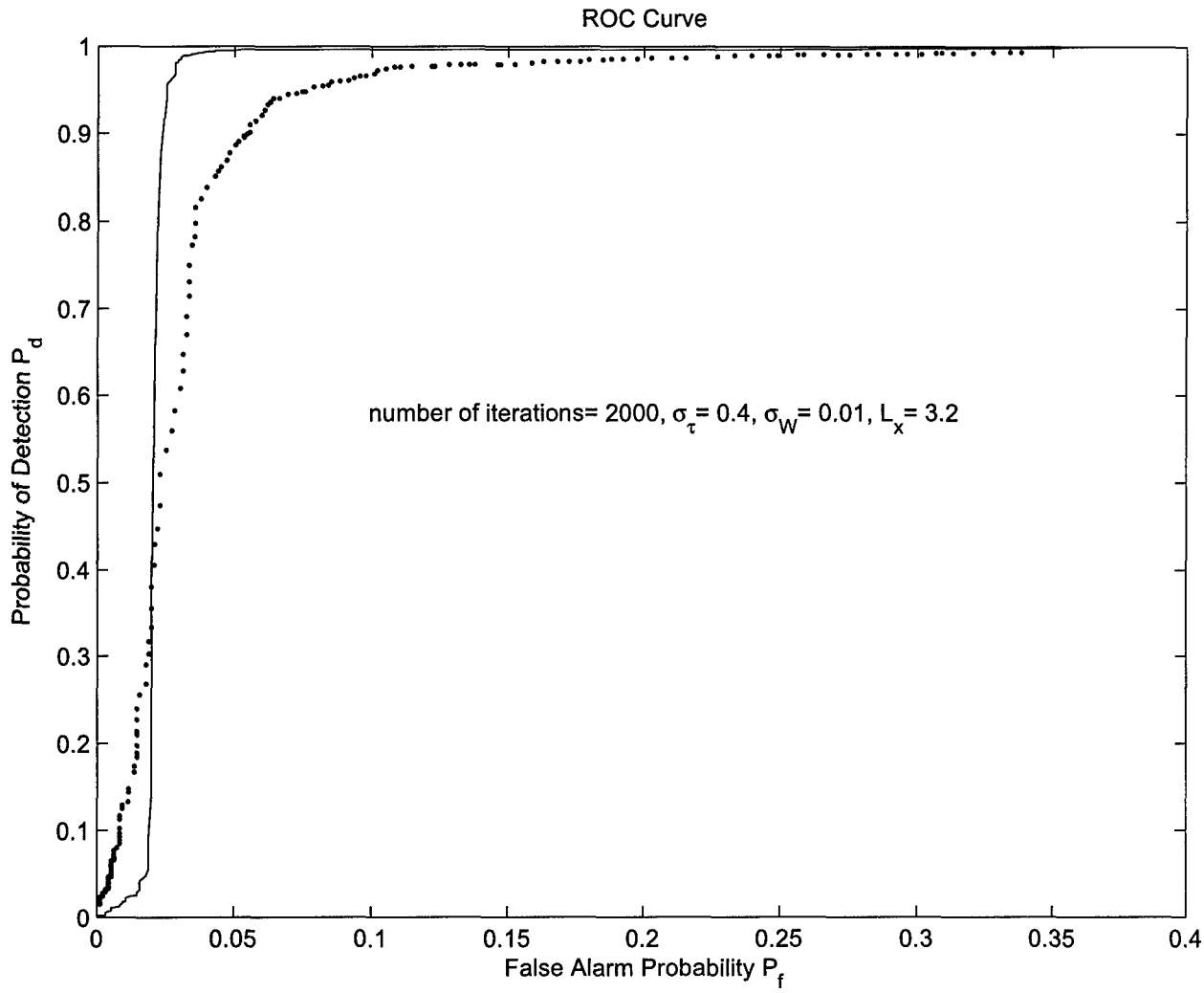

Figure 11: Receiver Operating Curves for the DWBA (dotted) and multiple scattering based (solid) algorithms.

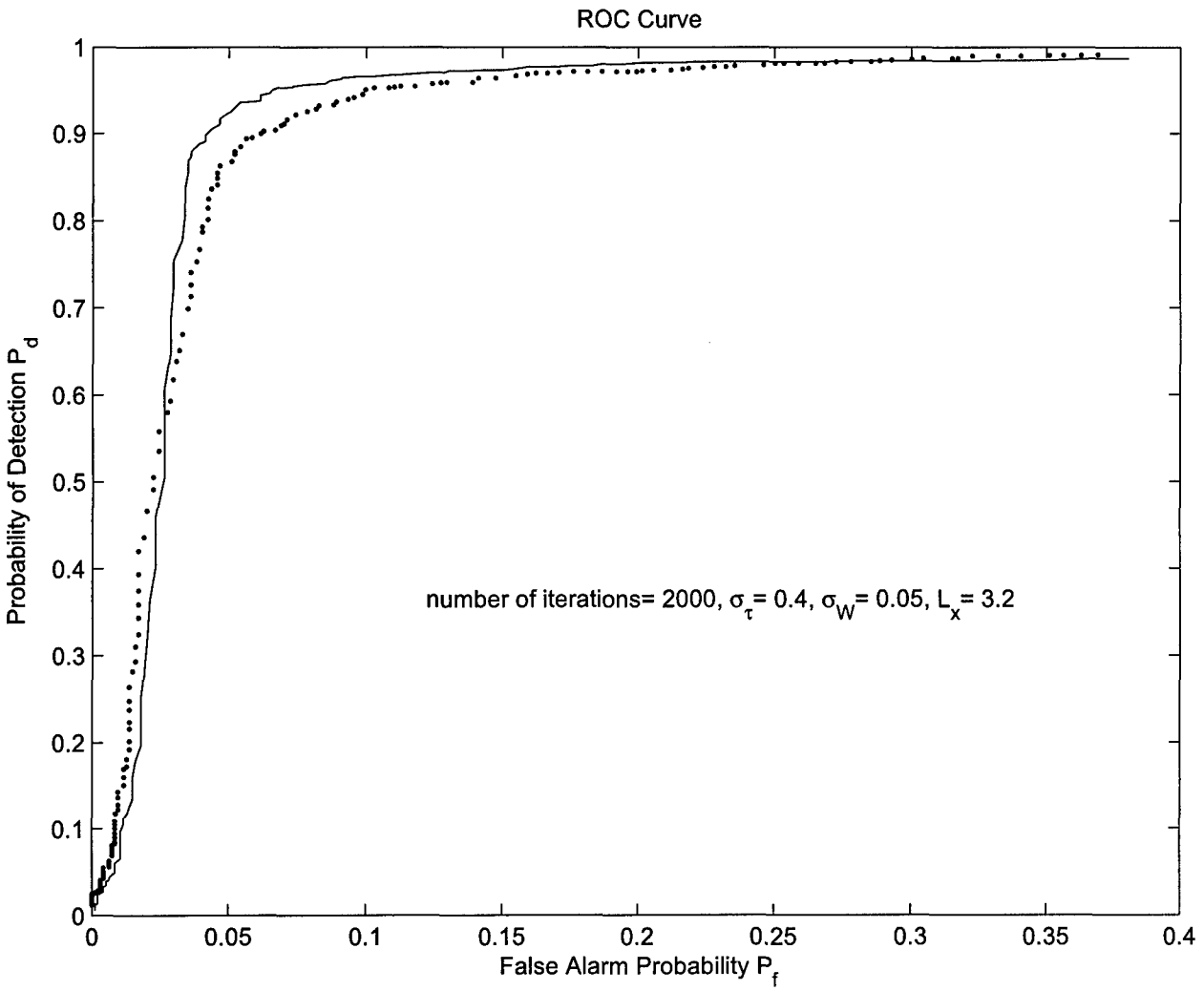

Figure 12: Receiver Operating Curves for the DWBA (dotted) and multiple scattering based (solid) algorithms.

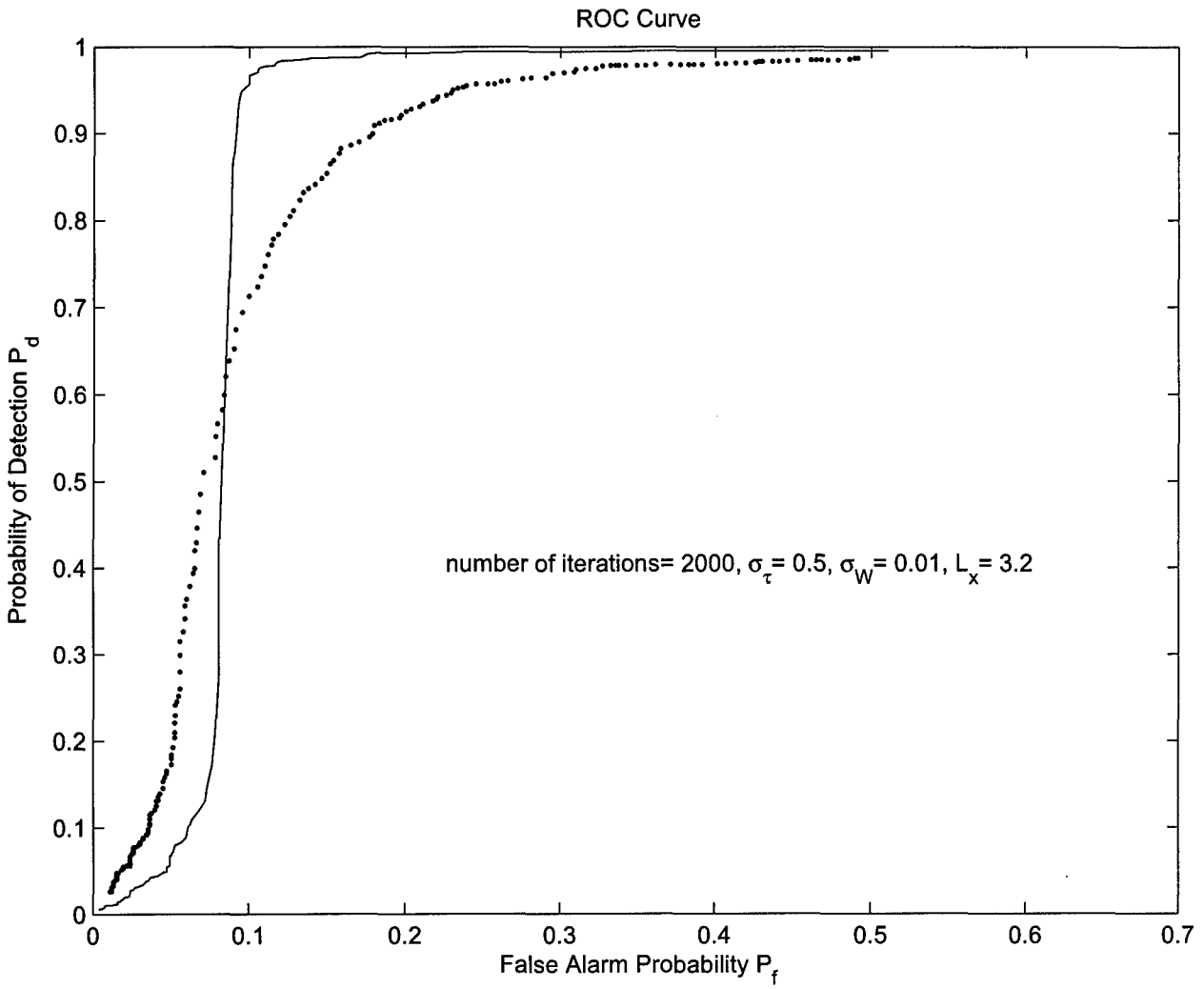

Figure 13: Receiver Operating Curves for the DWBA (dotted) and multiple scattering based (solid) algorithms.

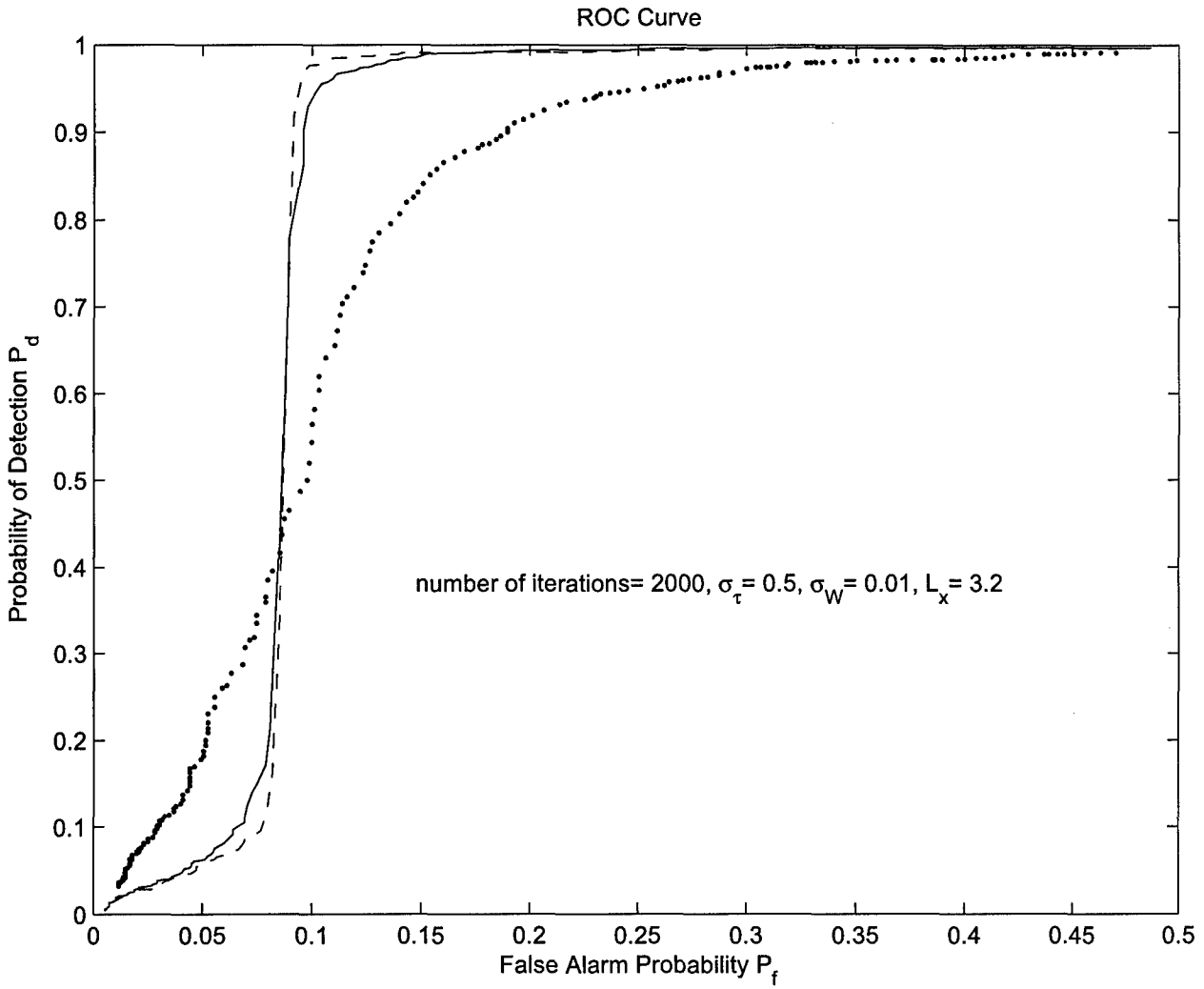

Figure 14: Receiver Operating Curves for the DWBA (dotted) and multiple scattering based (solid) algorithms.

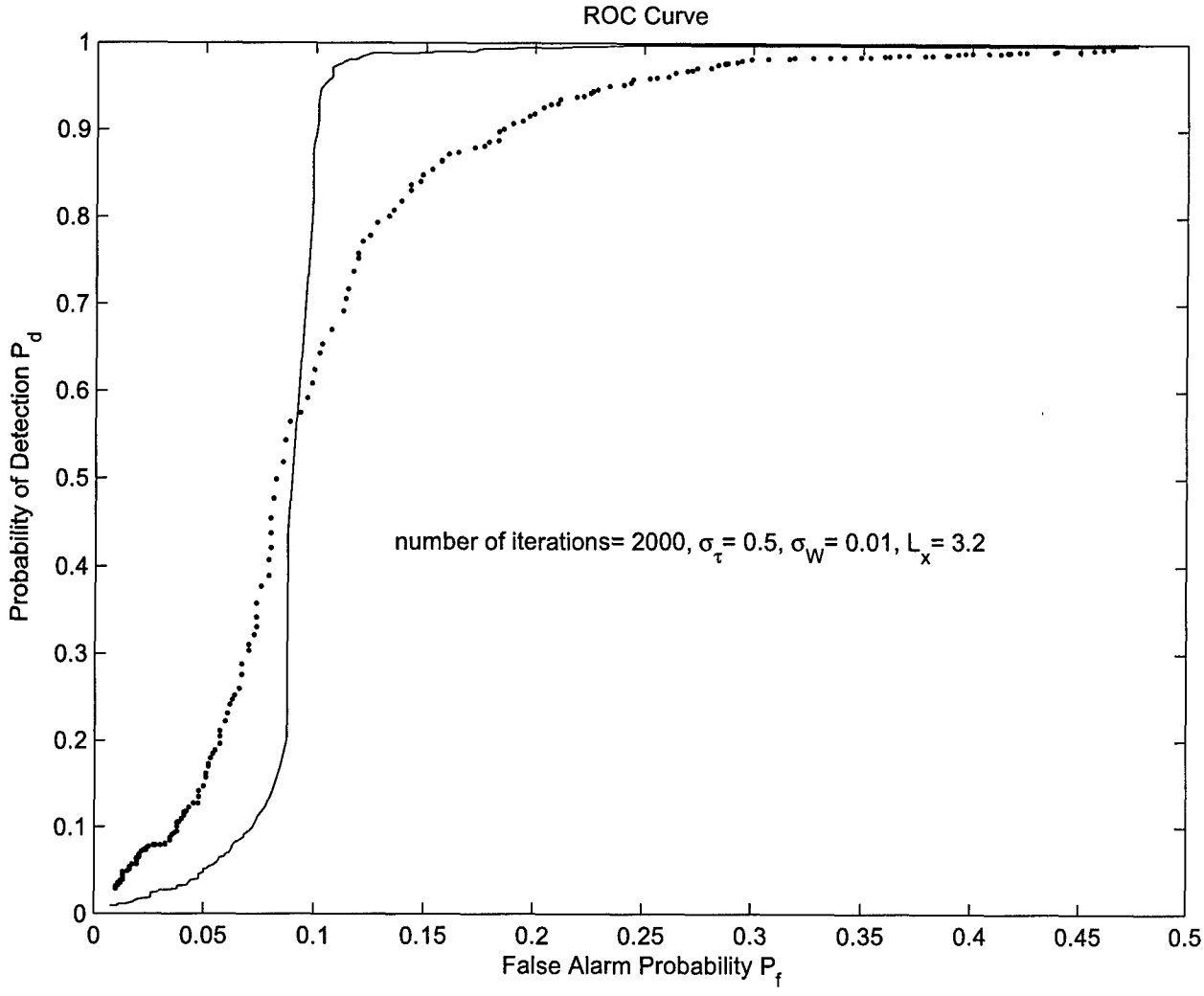

Figure 15: Receiver Operating Curves for the DWBA (dotted) and multiple scattering based (solid) algorithms.

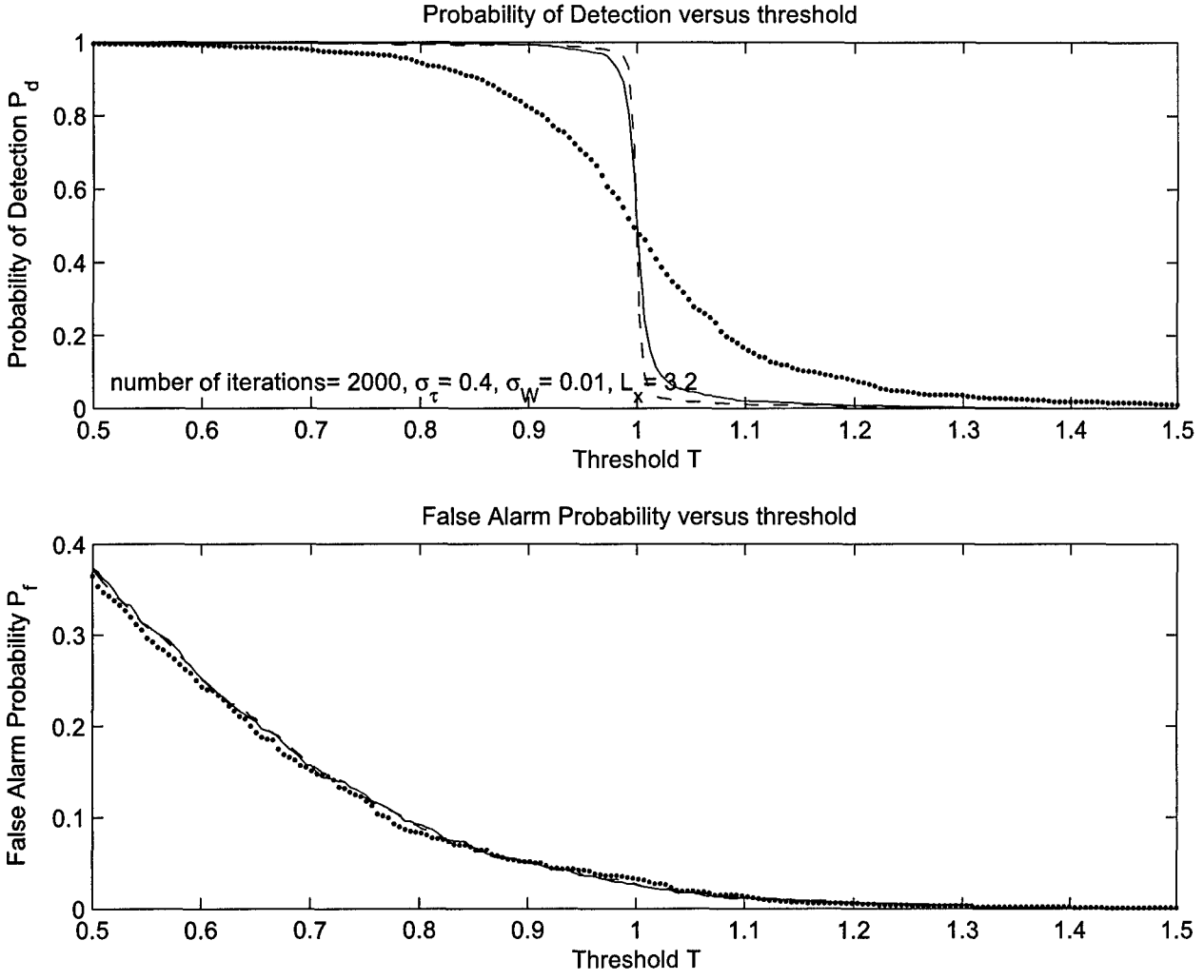

Figure 16: Plots of Probabilities of detection and false alarm for the DWBA (dotted) and multiple scattering based (solid) algorithms versus threshold value.

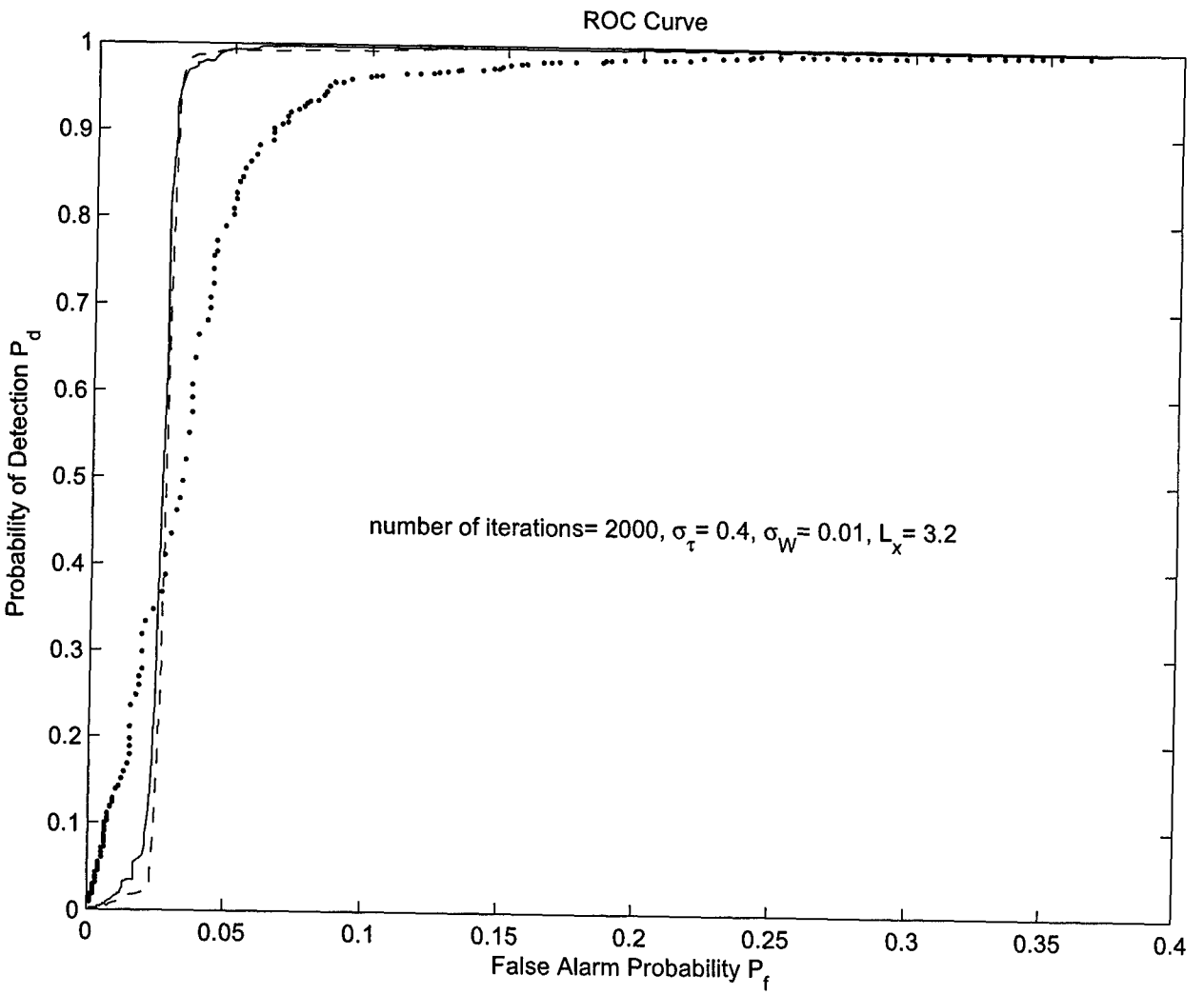

Figure 17: Receiver Operating Curves for the DWBA (dotted) and multiple scattering based (solid) algorithms.

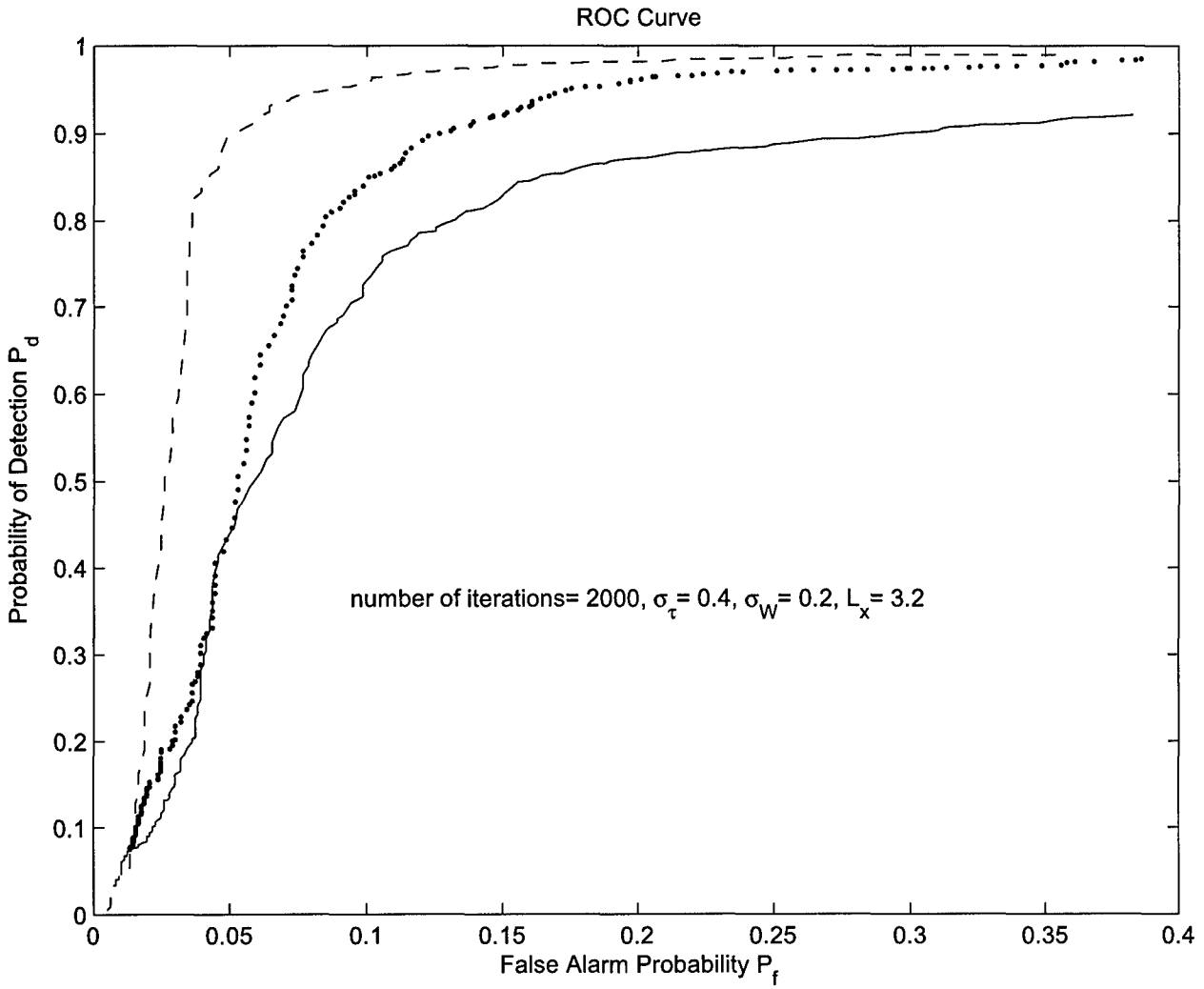

Figure 18: Receiver Operating Curves for the DWBA (dotted) and multiple scattering based (solid) algorithms.

target plus clutter K matrix is measured and that the clutter only K matrix is known and the detection problem then reduces to making a decision whether or not target is present from these data. The signal model for this detection problem can be expressed in the form

$$S_{j,k}(\omega_n) = \begin{cases} K^{s+c}_{j,k}(\omega_n) - K^{c}_{j,k}(\omega_n) + W_{j,k}(\omega_n) & H_1 \\ W_{j,k}(\omega_n) & H_0 \end{cases} \tag{10}$$

where $K^{s+c}_{j,k}$ is the experimentally obtained target plus clutter K matrix at 5 Ghz, $K^{c}_{j,k}$ is the experimentally obtained clutter only K matrix at this same frequency and $W_{j,k}$ is AWGN that is generated synthetically. Here, H_1 is the hypothesis that target is present and H_0 is the hypothesis that target is not present.

4.2 Detection Schemes

We used four detection schemes. The first was a benchmark that made its decision on the total signal energy:

$$\begin{cases} \text{choose } H_1 & \text{if } ||S_{j,k}|| > T \\ \text{choose } H_0 & \text{if } ||S_{j,k}|| < T \end{cases} \tag{11}$$

where T is a threshold that is varied to compute the ROC curves and $||\cdot||$ denotes the Frobenius norm of the matrix. The benchmark is a simple energy detection scheme and does not make use of any time reversal theory of methods.

The second scheme made its decision based on the maximum singular value of the signal matrix; i.e.,

$$\begin{cases} \text{choose } H_1 & \text{if } \sigma_1 > T \\ \text{choose } H_0 & \text{if } \sigma_1 < T \end{cases} \tag{12}$$

where σ_1 is the first (maximum) singular value of the matrix $S_{j,k}$. This scheme is in the spirit of time reversal since it uses the SVD of the measured K matrix.

The third scheme used the DORT image generated from the singular vector corresponding to the largest singular value of the $S_{j,k}$ matrix. In particular, the DORT image was generated and it maximum value was determined. The maximum value was normalized by the total energy of the Green function vectors at the image point and this statistic was compared with a detection threshold to arrive at the decision.

The final scheme was similar to the DORT scheme but used the *total time reversed image field* that is generated directly from the measured matrix $S_{j,k}$. This image field was discussed extensively in earlier reports and briefings. The maximum value of the total time reversed image field was normalized by the total energy of the Green function vectors at the image point and this statistic was compared with a detection threshold to arrive at the decision.

It is important to note that the last two schemes require that the location of the target be estimated from the data. The results of the study indicate that this is very important: the SVD of the K matrix is not enough. It is important to use a test statistic that is tied to the estimated value of the time reversed image fields at the target location.

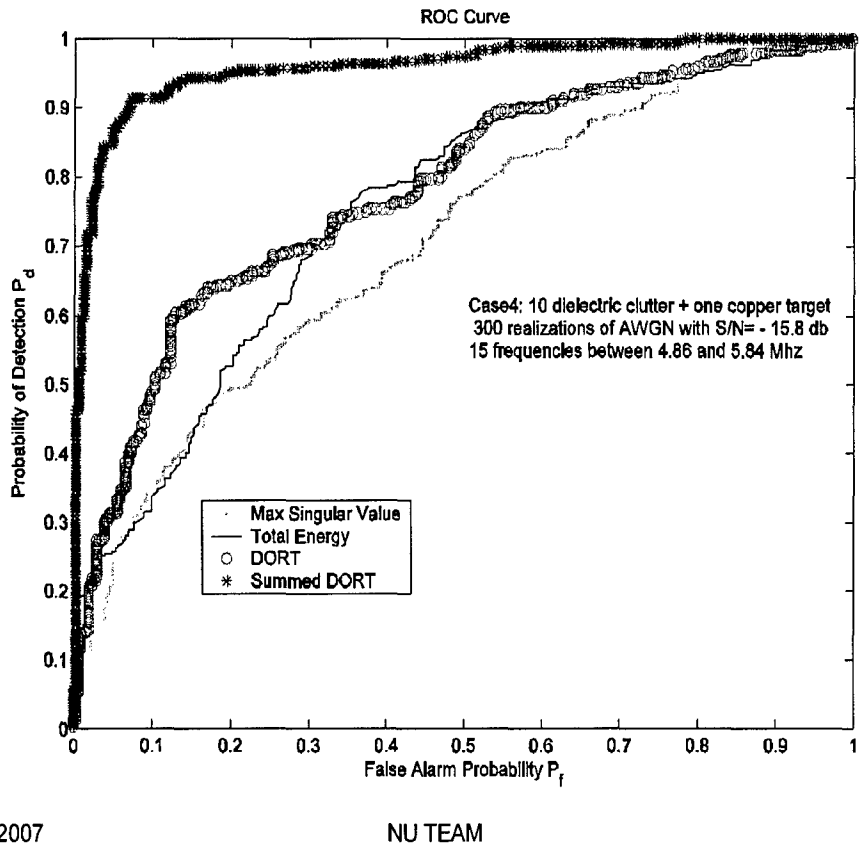

Figure 19: Real data simulation #1 from CMU experimental data.

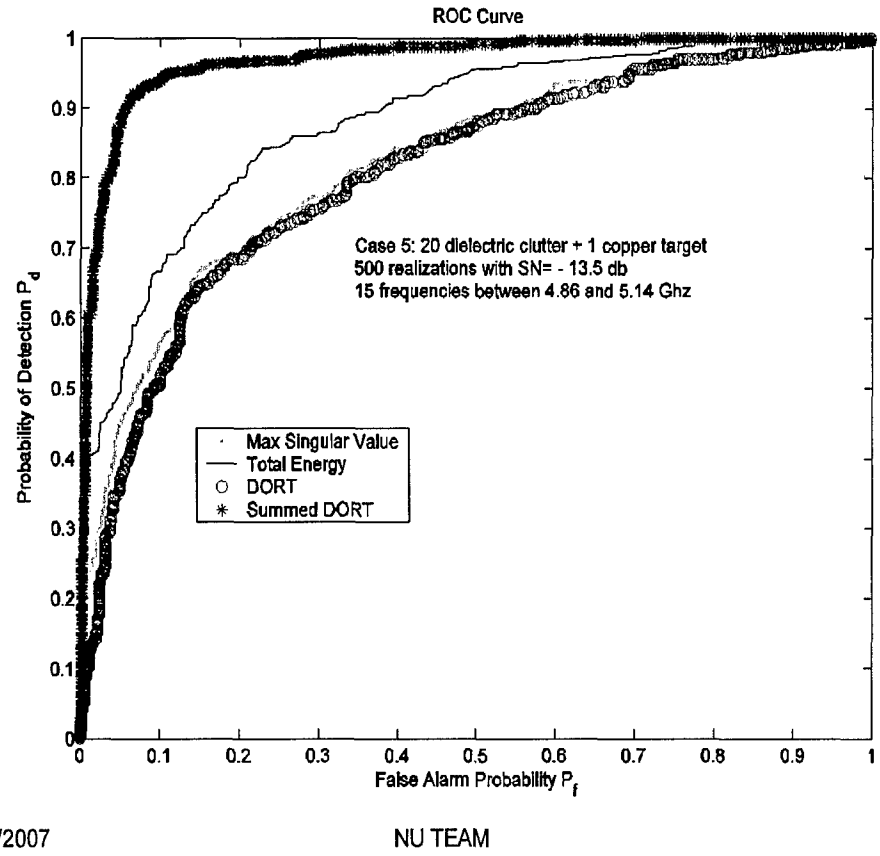

Figure 20: Real data simulation #2 from CMU experimental data.

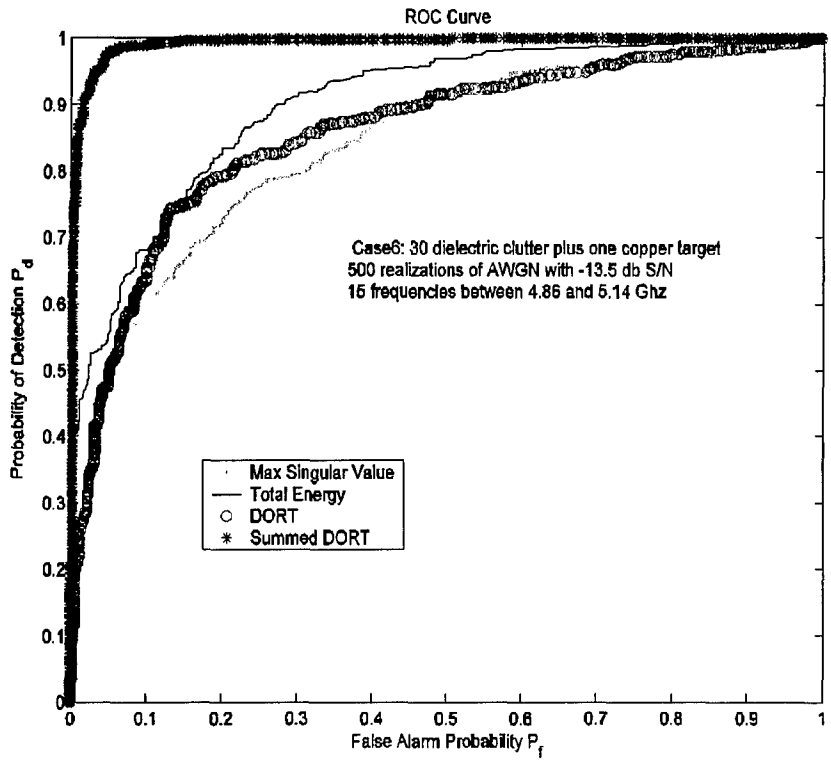

Figure 21: Real data simulation #3 from CMU experimental data.

5 Future Research

Whereas the research performed in this grant and reported herein concentrated on the detection of point targets in heavy clutter this research can be used as a basis for extended target imaging and inverse scattering applications. In particular, the generalized MUSIC algorithms developed in the program are readily extended to imaging of extended targets while the inverse scattering algorithms apply with virtually no change to these more general applications. Candidate applications for extension of the results obtained in the project include:

1. Imaging of ground targets using multistatic data collected from sets of UAV's,
2. Imaging in urban environments,
3. Imaging of hidden and unknown targets using acoustic data.

The above research goals are natural extensions of much of what has been performed in the program. Moreover, many of these goals were originally called for in the original NU DARPA proposal and much of the groundwork for completing these goals has already been laid in research already carried out in the project. The generalized MUSIC algorithms already developed in the project can be cast into a unified conceptual framework based on subspace weighting which is an ideal framework for achieving goal 1. This formulation leads naturally to a tried and true measure or performance based on the so-called *Point Spread Function* (PSF) of the imaging algorithms. Indeed, this measure of performance and the use of subspace weighting was the starting point of the famous Backus and Gilbert [14] classical work on geophysical data inversion. The performance of the inverse scattering algorithms can also be based on computed point spread functions as was done in [8, 9, 10]. These PSF's are functions of the measurement geometry, bandwidth and antenna radiation patterns and can be used to evaluate system parameters in terms of expected performance.

While the emphasis in goals 1 and 2 is on non-stochastic or "single snap shot" data, in Goal 3 the emphasis is on extending the theory and algorithms developed in the first two goals to a stochastic environment. Here, the performance of the algorithms would be based on statistical parameters such as the ensemble average PSF and the use of Cramer Rao performance bounds. Again much of the groundwork for this goal has been established in the project [12, 13]. Further extensions would include the development of statistically optimum ML estimation algorithms and robust estimation and imaging algorithms that are immune to un-certainties in the background Green function. This work would be closely tied to background Green function estimates generated in Goal 2; i.e., uncertainties in the computed Green function will be employed in the development of optimally immune imaging algorithms. Some preliminary statistical and robustness analysis has been done in the theses of Hanoch Lev-Ari's students Raha Zandifar (MS, 2001) and Minhtri Ho (PhD, 2005), including peak shape for TR-MUSIC, effect of additive noise on location estimates, and statistics of singular values. Much more remains to be done, especially in the context of non-ideal wave propagation and non-isotropic antenna elements.

References

[1] L.L. Foldy, 'The multiple scattering of waves," *Physical Review* , **67**, pp.107-119 (1945).

[2] F.K. Gruber, E.A. Marengo, and A.J. Devaney, "Time-reversal imaging with multiple signal classification considering multiple scattering between the targets," *J. Acoust. Soc. Am.* **115**, 3042-3047 (2004).

[3] H. Lev-Ari and A.J. Devaney, "The time-reversal technique re-interpreted: Subspace-based signal processing for multi-static target location", *IEEE Sensor Array and Multichannel Signal Processing Workshop*, Cambridge, MA, 2000, pp. 509-513.

[4] S. Lehman and A.J. Devaney, "Transmission mode time-reversal super-resolution imaging", *J. Acoust. Soc. Am.* **113**, 2742-2753 (2003).

[5] A.J. Devaney, E.A. Marengo, and F.K. Gruber, "Time-reversal based imaging and inverse scattering of multiply scattering point targets," *J. Acoust. Soc. Am.* **118**, No. 5, Nov. 2005, pp. 3129-3138.

[6] A.J. Devaney and H. Lev-Ari, "A Monte Carlo simulation study of time reversal imaging and detection of a point target in heavy clutter," in preparation.

[7] A.J. Devaney, H. Lev-Ari, Ahmet Cepni, Ben Henti, and Dan Stancil,"Electromagnetic Time Reversal Imaging of Systems of Point Targets," in preparation.

[8] A.J. Devaney and M. Dennison, "Inverse scattering in inhomogeneous background media," *Inverse Problems* **19** (2003).

[9] M.Dennison and A.J. Devaney, "Inverse scattering in inhomogeneous background media: II Multi frequency case and SVD formulation, *Inverse Problems* **20** (2004).

[10] Y. Fei and A.J. Devaney, "Inverse scattering for real valued scattering potentials," *Inverse Problems* **21** (2005).

[11] M. Mordant, C. Prada and M. Fink, "Highly resolved detection and selective focusing in a waveguide using the D.O.R.T. method", *J. Acoust. Soc. Am.* **105**, 2634-2642 (1999).

[12] G. Shi and A. Nehorai, "Maximum likelihood estimation of point scatterers for computational time-reversal imaging," to appear in *Communications in Information and Systems.*

[13] G. Shi and A. Nehorai, "Maximum likelihood estimation of point scatterers for computational time-reversal imaging," in *Proc. 13th Annu. Workshop on Adaptive Sensor Array Processing,* Lincoln Laboratory, MIT, Lexington, MA, June 2005.

[14] Backus, G.E., and Gilbert, F.*Geophysical Journal of the Royal Astronomical Society,* **16**, pp. 169205 (1968)

[15] A.J. Devaney, "Time reversal imaging of obscured targets from multistatic data," *IEEE Trans Ant & Prop* **53** (2005).